

Light quark Yukawas in triboson final states

Adam Falkowski,¹ Sanmay Ganguly,² Philippe Gras,³ Jose Miguel No,^{4,5} Kohsaku Tobioka,^{6,7} Natascia Vignaroli,⁸ Tevong You^{9,10}

¹*Université Paris-Saclay, CNRS/IN2P3, IJCLab, 91405 Orsay, France*

²*Department of Particle Physics & Astrophysics, Weizmann Institute of Science, Israel*

³*CEA Institut de Recherche sur les lois Fondamentales de l'Univers, Université Paris-Saclay, Gif-sur-Yvette, France*

⁴*Departamento de Física Teórica, Universidad Autónoma de Madrid, 28049, Madrid, Spain*

⁵*Instituto de Física Teórica, IFT-UAM/CSIC, Cantoblanco, 28049, Madrid, Spain*

⁶*Department of Physics, Florida State University, Tallahassee, FL 32306, USA*

⁷*High Energy Accelerator Research Organization (KEK), Tsukuba 305-0801, Japan*

⁸*Dipartimento di Fisica "E. Fermi", Università di Pisa, and INFN Pisa, Largo Bruno Pontecorvo 3, 56127 Pisa, Italy*

⁹*CERN, Theoretical Physics Department, Geneva, Switzerland*

¹⁰*DAMTP, University of Cambridge, Wilberforce Road, Cambridge, CB3 0WA, UK; Cavendish Laboratory, University of Cambridge, J.J. Thomson Avenue, Cambridge, CB3 0HE, UK*

ABSTRACT: Triple heavy vector boson production, $pp \rightarrow VVV$ ($V = W, Z$), has recently been observed for the first time. We propose that precision measurements of this process provide an excellent probe of the first generation light quark Yukawa couplings. Modified quark interactions with the off-shell Higgs in this process lead to a rapid growth of the partonic cross sections with energy, which manifests in an enhanced p_T distribution of the final state leptons and quarks. We quantify this effect and estimate the present and future 2σ sensitivity to the up, down, and strange Yukawas. In particular, we find that HL-LHC can reach $\mathcal{O}(400)$ sensitivity to the down Yukawa relative to the Standard Model value, improving the current sensitivity in this process by a factor of 10, and which can be further improved to $\mathcal{O}(30)$ at FCC-hh. This is competitive with and complementary to constraints from global fits and other on-shell probes of the first generation Yukawas. The triboson sensitivity at HL-LHC corresponds to probing dimension-6 SMEFT operators suppressed by an $\mathcal{O}(1)$ TeV scale, similarly to other LHC Higgs probes.

Contents

1	Introduction	1
2	Theoretical framework	3
3	Triple heavy vector boson channels	6
3.1	<i>WWW</i> : same-sign di-lepton final state	7
3.2	<i>WWW</i> : three-lepton final state	10
3.3	<i>ZZZ</i> : four-lepton final state	12
3.3.1	$4\ell + E_T^{\text{miss}}$	12
3.3.2	$4\ell + 2j$	15
4	Comparison with other constraints	16
5	Conclusion	17

1 Introduction

The Higgs mechanism plays a central role in the Standard Model (SM). It leads to spontaneous breaking of the electroweak (EW) symmetry, giving masses to the W and Z bosons, and at the same time it generates masses for the SM quarks and leptons. One important prediction is the existence of a scalar particle—the Higgs boson—whose Yukawa interactions with each SM fermion have their strength proportional to the fermion’s mass. Precision studies of the Higgs boson at the LHC are providing spectacular confirmation of this prediction. We currently have firm evidence [1, 2] that the Higgs couples to the 3rd generation fermions (top, bottom, tau) with the strength predicted by the SM, within $\mathcal{O}(10\%)$ accuracy. There is also preliminary evidence for the Higgs decays to muons [3, 4], which is the first experimental verification of the SM Higgs mechanism at the level of the 2nd generation fermions.

Higgs decays to 1st and 2nd generation quarks are much more difficult to determine experimentally. If the SM predictions concerning their magnitude are borne out in nature, it will be very challenging to pinpoint their signatures in current or future hadron colliders. However, the SM predictions should not be taken for granted. The pattern of observed fermion masses is mysterious, which prompts many theorists to suspect a deeper explanation involving new physics beyond the SM. That new physics might dramatically alter the Higgs boson couplings to the light quarks. In the absence of deeper theoretical understanding, it is essential to continue sharpening the experimental picture with the help of novel analysis strategies and techniques.

The literature already contains several theoretical ideas to better aim at the Higgs coupling to the charm [5–10] and/or lighter [7, 11–19] quarks, and several targeted analyses

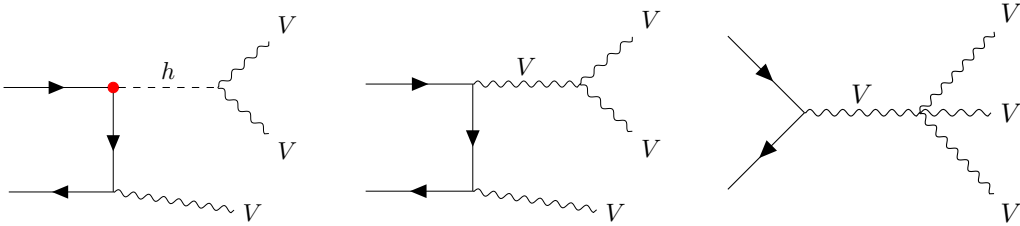


Figure 1. Illustrative tree-level Feynman diagrams in the unitary gauge contributing to the triple electroweak gauge boson production, $f\bar{f} \rightarrow VVV$. In the SM, the Higgs exchange diagrams (left) cancel the bad high-energy behavior of the remaining diagrams to ensure that $\sigma(f\bar{f} \rightarrow VVV)$ does not grow with the center-of-mass energy.

by the LHC collaborations have appeared [20–25]. These have so far relied on processes with on-shell Higgs boson(s). We propose an alternative probe, where the Higgs boson appears only as an intermediate off-shell particle in triboson production processes. Our approach is in line with the programme of *measuring Higgs couplings without Higgs bosons* laid out in Ref. [26]. Indeed, the SM multi-boson processes and Higgs physics are intricately intertwined by the delicate cancellations necessary to avoid violation of perturbative unitarity in the high-energy behavior of scattering amplitudes. Beyond the SM (BSM), when that cancellation is disrupted, the multi-boson cross sections may rapidly grow with the center-of-mass energy of the collision, thus amplifying the effect of the non-SM perturbation. Experimental searches for such energy-growing effects allow one to identify or constrain possible deviations of Higgs couplings from their SM values. In particular, they provide a novel handle on the Higgs Yukawa couplings to light quarks—up, down, and strange—as we argue in this paper.

Specifically, we study here the triple EW gauge boson production in hadron colliders, $pp \rightarrow VVV$, where V stands for an on-shell W or Z gauge boson. This process was recently observed for the first time by the CMS collaboration [27, 28]. At the partonic level it is dominated by $q\bar{q} \rightarrow VVV$, which receives a contribution from the diagram with an intermediate Higgs, see Fig. 1. That diagram plays a crucial role in controlling the high-energy behavior of the amplitude, and any deviations of the $h\bar{q}q$ (and hVV) couplings from the SM value lead to the $q\bar{q} \rightarrow VVV$ cross-section growing quadratically with energy. In this work we show that this effect allows one to obtain competitive constraints on the Higgs Yukawa couplings to the up, down and strange quarks.¹

In the next Section we introduce our theoretical framework and notation for modified Yukawa couplings. In Section 3 we study the 2-, 3-, and 4-lepton final states and backgrounds of triple EW gauge boson production and estimate their sensitivity to modified up, down and strange Yukawa couplings. The comparison with other constraints on the same couplings is discussed in Section 4, before concluding in Section 5.

¹The same process also probes the charm and bottom Yukawa couplings, but in this case the effect is suppressed by the small c and b parton distribution functions (PDFs) inside the proton. Therefore the resulting constraints are inferior to those obtained from other more direct probes, and we do not discuss them in this paper.

2 Theoretical framework

We work in the framework of the SM effective field theory (SMEFT), in which the SM Lagrangian is supplemented with a set of gauge-invariant higher-dimensional operators built from the SM fields. The latter encode possible effects of heavy BSM particles on the phenomenology at the EW scale. In this work we will focus on a specific subset of dimension-6 operators:

$$\mathcal{L}_{\text{SMEFT}} \supset \frac{Y_u |H|^2}{v^2} \bar{u}_R Q_{1,L} H + \frac{Y_d |H|^2}{v^2} \bar{d}_R H^\dagger Q_{1,L} + \frac{Y_s |H|^2}{v^2} \bar{s}_R H^\dagger Q_{2,L} + \text{h.c.}, \quad (2.1)$$

where $Q_{1,L} = (u_L, d_L)$ and $Q_{2,L} = (c_L, s_L)$ are the left-handed 1st and 2nd generation SM quark doublets, H is the Higgs doublet, and $v \approx 246.22$ GeV is its VEV. We assume that the parameters Y_q are real, for simplicity. The operators in (2.1) are generated e.g. by integrating out heavy vector-like quarks with masses of order $v/\sqrt{|Y_q|}$ and mixing with the light SM quarks after EW symmetry breaking. In restricting to this set of operators, we hereby assume that these give the dominant non-SM contribution to Higgs phenomenology, and neglect possible effects of other dimension-6 operators. The Higgs doublet can be parametrized as

$$H = \frac{1}{\sqrt{2}} \begin{pmatrix} i\sqrt{2}G_+ \\ v + h + iG_z \end{pmatrix}, \quad (2.2)$$

where h is the Higgs boson field, and G_i are unphysical Goldstone bosons eaten by the W and Z gauge bosons. By virtue of the equivalence theorem [29], the Goldstone bosons can be in a certain sense identified with the longitudinal polarisations of the W and Z bosons for processes with a characteristic energy scale $E \gg m_Z$. This point will prove key to understand the phenomena discussed in this work.

The SMEFT provides a very convenient framework for understanding correlations between various new physics effects. In particular, each of the higher-dimensional operators in (2.1) simultaneously contributes to several observables, such as the Higgs signal strength, double Higgs production, triple EW gauge boson production, etc. In the following of this section we will show how the modified $h\bar{q}q$ couplings and the high-energy behavior of the $pp \rightarrow VVV$ cross section are correlated.²

Let us first discuss the relation between the operators in Eq. (2.1) and the coupling strength between the Higgs boson and the light quarks. We parametrize these Yukawa couplings as

$$\mathcal{L} \supset -\frac{h}{v} \sum_{q=u,d,s} m_q (1 + \delta y_q) \bar{q}q. \quad (2.3)$$

The relative shifts of the Yukawa couplings with respect to the SM values are encoded in the parameters δy_q . They are related to the parameters in Eq. (2.1) by

$$\delta y_q = -\frac{Y_q}{y_q^{\text{SM}}}, \quad (2.4)$$

²We note in passing that the same operators also lead to an energy-growing behaviour of the $pp \rightarrow WWqj$ cross section. The sensitivity of that process to the charm Yukawa was previously studied in Ref. [30], and to the top Yukawa coupling in Refs. [26, 30, 31]. See also Ref. [32] for a related process with the linear energy growth.

	u	d	s	c	b
$m_q(m_h)$ GeV	0.0013(1)	0.0027(1)	0.0524(4)	0.616(4)	2.804(8)
y_q^{SM}	7.5×10^{-6}	1.5×10^{-5}	3.0×10^{-4}	3.5×10^{-3}	1.6×10^{-2}
$\text{Br}(h \rightarrow q\bar{q})_{\text{SM}}$	1.3×10^{-7}	5.5×10^{-7}	2.1×10^{-4}	2.9×10^{-2}	0.58

Table 1. Quark masses and SM Yukawa coupling values at the Higgs mass scale. These have been obtained using the input values at $\mu = 2$ GeV: $m_u = 2.3(1)$ MeV, $m_d = 4.7(1)$ MeV, $m_s = 92.9(7)$ MeV [33], as well as $m_c(3 \text{ GeV}) = 0.988(7)$ GeV, $m_b(m_b) = 4.198(12)$ GeV [34]. These have then been evolved up to $\mu = m_h$ using the 4-loop QCD running equations [35, 36] together with the 5-loop running α_s [37] and $\alpha_s(m_Z) = 0.1179(10)$ [33].

with the SM Yukawa coupling defined as $y_q^{\text{SM}} \equiv \sqrt{2}m_q/v$. In all of the following we will use y_q^{SM} evaluated at the Higgs mass scale³, that is to say, calculated using the quark masses evolved up to the renormalization scale $\mu = m_h$. The quantity $m_q(m_h)$ differs by an $\mathcal{O}(2)$ factor from the low-energy value of the corresponding quark mass. The numerical values of $m_q(m_h)$ and y_q^{SM} for light quarks are summarized in Table 1.

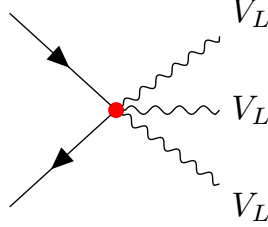


Figure 2. The Feynman diagram in the non-unitary gauge that gives the dominant contribution to the $\mathcal{M}(q\bar{q} \rightarrow GGG)$ amplitude at large center-of-mass energies \sqrt{s} . By the equivalence theorem, this amplitude is approximately equal to the amplitude for production of longitudinally polarized EW gauge bosons, $\mathcal{M}(q\bar{q} \rightarrow V_L V_L V_L)$ in the energy range $\sqrt{s} \gg m_Z$.

We move to discussing the connection between the operators in Eq. (2.1) and the triple EW gauge boson production. As we discussed in Introduction, as soon as $\delta y_q \neq 0$, the Higgs exchange diagram in Fig. 1 no longer regulates the bad high-energy behavior of the remaining diagrams, leading to the quadratic energy growth of the $q\bar{q} \rightarrow VVV$ cross section. There is a more transparent way to see it starting from (2.1) and taking advantage of the equivalence theorem. Inserting the H parametrization of Eq. (2.2) into Eq. (2.1) leads to the contact interactions between two quarks and three Goldstone bosons:

$$\begin{aligned}
\mathcal{L} \supset & \frac{1}{v^2} \left(G_+ G_- + \frac{1}{2} G_z^2 \right) \left\{ i y_u^{\text{SM}} \delta y_u \left(\sum_{q'=d,s} \bar{u}_R q'_L G_+ - \bar{u}_R u_L \frac{G_z}{\sqrt{2}} \right) \right. \\
& \left. + i \sum_{q'=d,s} y_{q'}^{\text{SM}} \delta y_{q'} \left(\bar{q}'_R u_L G_- + \bar{q}'_R q'_L \frac{G_z}{\sqrt{2}} \right) + \text{h.c.} \right\}. \quad (2.5)
\end{aligned}$$

³We note that, since we will be interested in off-shell Higgs processes, the relevant energy scale μ at which y_q^{SM} should be evaluated is typically larger than m_h , but the renormalization group evolution from m_h to the actual scale probed by the differential distribution generally has a very small impact relative to current uncertainties [38].

These interactions are relevant for the $\mathcal{M}(q\bar{q} \rightarrow GGG)$ amplitude which, by the equivalence theorem, approximates the high-energy behavior of the $\mathcal{M}(q\bar{q} \rightarrow VVV)$ amplitude. By dimensional analysis, they contribute as $\mathcal{M}(q\bar{q} \rightarrow GGG) \sim \mathcal{O}(\delta y_q E/v^2)$ for $E \gg m_q$, where E is the center-of-mass energy of the process. Other tree-level diagrams affecting the same process are more suppressed at high energies because they contain internal propagators. Thus, whenever $\delta y_q \neq 0$, the diagram in Fig. 2 represents the dominant contribution to $\mathcal{M}(q\bar{q} \rightarrow GGG)$ at high energies. Note that, in this picture, the high-energy behavior is controlled by a *single* diagram. This is a qualitative simplification compared to the calculation in the unitary gauge, where this high-energy behavior depends on an interplay between several diagrams in Fig. 1. Of course, both calculations are guaranteed to yield the same result, as a consequence of the gauge invariance of the SMEFT.

Treating the quarks and Goldstone bosons as massless, the cross sections for the $q\bar{q} \rightarrow GGG$ processes mediated by the interactions in Eq. (2.5) are given by the simple analytic expressions

$$\begin{aligned}\sigma(q\bar{q} \rightarrow G_z G_+ G_-) &= (y_q^{\text{SM}} \delta y_q)^2 I(\hat{s}), & I(\hat{s}) &\equiv \frac{\hat{s}}{6144\pi^3 v^4}, \\ \sigma(q\bar{q} \rightarrow 3G_z) &= \frac{3}{2} (y_q^{\text{SM}} \delta y_q)^2 I(\hat{s}), \\ \sigma(u\bar{q}' \rightarrow G_+ G_z G_z) + \sigma(q'\bar{u} \rightarrow G_- G_z G_z) &= \frac{1}{2} [(y_u^{\text{SM}} \delta y_u)^2 + (y_{q'}^{\text{SM}} \delta y_{q'})^2] I(\hat{s}), \\ \sigma(u\bar{q}' \rightarrow G_+ G_+ G_-) + \sigma(q'\bar{u} \rightarrow G_- G_- G_+) &= 2 [(y_u^{\text{SM}} \delta y_u)^2 + (y_{q'}^{\text{SM}} \delta y_{q'})^2] I(\hat{s}),\end{aligned}\quad (2.6)$$

with $q = u, d, s$ and $q' = d, s$, and $\sqrt{\hat{s}}$ is the centre-of-mass energy of the parton level quark-antiquark collision. By the equivalence theorem, these expressions approximate the parton-level triple EW gauge boson cross sections for $\sqrt{\hat{s}} \gg m_Z$, with the identification $G_z \rightarrow Z_L$ and $G_\pm \rightarrow W_L^\pm$.

We can readily make a number of observations that will be important for the subsequent collider analysis:

(i) As expected from the above general arguments, for $\delta y_q \neq 0$ the cross section in all channels grows quadratically with the centre-of-mass energy of the partonic collision. On the other hand, in the SM the triple EW gauge boson cross section is instead suppressed at high energies. Therefore, selecting VVV events with large $\sqrt{\hat{s}}$ will enhance the sensitivity to $\delta y_q \neq 0$.

(ii) The dimension-6 operators in Eq. (2.1) lead to a characteristic signal pattern in different VVV channels, distinct from the pattern predicted by in the SM or by new physics manifesting itself via anomalous triple gauge boson couplings. In case of an excess over the SM in VVV signatures, observation of the signal in multiple channels would allow one to identify the scenario responsible for it.

(iii) In connection to the previous point, the signal in different VVV channels depends on the different combinations of the Yukawa corrections δy_u , δy_d and δy_s . In particular, from (2.6) it is clear that for the charge ± 1 final states ($W^\pm W^\pm W^\mp$ and $W^\pm ZZ$) the cross-section enhancement is the same for δy_u or δy_d modifications, and does not allow to

HL-LHC	SM	BSM ($Y_d = 1$)	BSM ($Y_u = 1$)	BSM ($Y_s = 1$)
$W^+W^-W^+$	152 fb	3.6 pb	3.6 pb	110 fb
$W^+W^-W^-$	87 fb	1.5 pb	1.5 pb	110 fb
ZZW^+	40 fb	1.0 pb	1.0 pb	31 fb
ZZW^-	23 fb	0.43 pb	0.43 pb	31 fb
ZW^+W^-	191 fb	1.5 pb	2.4 pb	120 fb
ZZZ	16 fb	0.99 pb	1.7 pb	66 fb

FCC-hh	SM	BSM ($Y_d = 1$)	BSM ($Y_u = 1$)	BSM ($Y_s = 1$)
$W^+W^-W^+$	2.35 pb	290 pb	290 pb	16 pb
$W^+W^-W^-$	1.76 pb	140 pb	140 pb	16 pb
ZZW^+	756 fb	74 pb	74 pb	4.4 pb
ZZW^-	579 fb	36 pb	36 pb	4.4 pb
ZW^+W^-	3.93 pb	94 pb	150 pb	12 pb
ZZZ	231 fb	110 pb	180 pb	11 pb

Table 2. Values of different triboson production cross sections for $\sqrt{s} = 14$ TeV LHC (upper table) and $\sqrt{s} = 100$ TeV FCC-hh (lower table) for the SM (computed at NLO in QCD [39, 40]) and with the addition of the dimension-6 operators from Eq. (2.1), with $Y_d = 1$ (with $Y_{\neq d} = 0$), $Y_u = 1$ (with $Y_{\neq u} = 0$) and $Y_s = 1$ (with $Y_{\neq s} = 0$), respectively. These latter cross sections are computed at LO.

distinguish between both. In contrast, for the neutral final states (ZW^+W^- and ZZZ), the different partonic content of up and down quarks in the proton leads to different cross-section enhancements for δy_u and δy_d . This is shown explicitly in Table 2 (which is based on complete calculations, rather than the Golstone boson approximation at high-energies). Assuming $\delta y_s = 0$, observation of a combined excess in neutral and charge ± 1 VVV channels would allow one to disentangle δy_u from δy_d .

(iv) Finally, we note that this observable is different from probes involving on-shell Higgs bosons, since the set of operators that can modify the Higgs boson production and decay patterns is much larger than for triboson.

3 Triple heavy vector boson channels

In this Section we analyse in detail the sensitivity of triple EW gauge boson production to the light quark Yukawa modifications parametrized by δy_u , δy_d and δy_s . We will focus on the HL-LHC with $\sqrt{s} = 14$ TeV and a future FCC-hh collider with $\sqrt{s} = 100$ TeV. In our analysis we will assume, for simplicity, that only one of these modifications is present at a time. However we note that combining several triboson channels allows one, in principle, to disentangle the different δy_q .

We begin by showing in Table 2 the various triboson production cross-sections, $\sigma(pp \rightarrow VVV)$, at the LHC and FCC-hh, turning on one BSM Yukawa contribution from Eq. (2.1) at a time. The cross-sections for the SM are computed at NLO in QCD [39, 40]. The BSM cross-sections are dominated by the quadratic contribution since the interference

between SM and BSM contributions is proportional to the SM Yukawa coupling of the light quarks and thus negligible. We use `MadGraph5_aMC@NLO` [41] using the NNPDF 2.3 PDF set for our simulations. We implemented the relevant BSM interactions from (2.3) in the unitary gauge using `Feynrules` [42]. From Table 2, we see that the triboson channel, which presents the largest cross section enhancement with respect to the SM, is by far $pp \rightarrow ZZZ$. Given sufficient luminosity it could be the most sensitive channel and, due to the smallness of the signal in the SM, a smoking gun for new physics. Final state leptons reconstructing the Z also provide a clean final state at a hadron collider. However, the smaller cross-section for this channel compared to others particularly due to the small Z boson branching fraction into leptons, will limit considerably the final sensitivity. On the other hand, the $pp \rightarrow W^\pm W^\pm W^\mp$ channel has the largest triboson production cross section, which also makes it key for our sensitivity analysis. The $W^+W^-W^\pm$ and ZZZ production will be the two channels we will target in our sensitivity analysis below, bearing in mind that the addition of the remaining channels in Table 2 would further increase the sensitivity to δy_q in triboson processes. In the next subsections we consider in turn the WWW and ZZZ channels.

3.1 WWW : same-sign di-lepton final state

The same-sign leptonic channel corresponds to the process $pp \rightarrow W^\pm W^\pm W^\mp \rightarrow \ell^\pm \ell^\pm \nu \nu jj$, with $\ell \equiv e, \mu$. We start by considering the recent 13 TeV CMS search for triple gauge boson production with 137 fb^{-1} [27, 43], that can already be used to put a limit on δy_q , choosing δy_d first as an example. The $pp \rightarrow WWW \rightarrow \ell^\pm \ell^\pm \nu \nu jj$ signal cross section as a function of Y_d is approximately given by

$$\sigma(Y_d) = 7.5 \text{ fb} + Y_d^2 \times 210 \text{ fb}, \quad (3.1)$$

where we have omitted the negligible interference term. The SM cross section is given at NLO in QCD [39], and we have multiplied the BSM signal cross section obtained from `MadGraph5_aMC@NLO` by an NLO k -factor, $k = 1.28$ [18]. According to the CMS analysis, the $\mu^\pm \mu^\pm$ and $e^\pm \mu^\pm$ final states in the “ m_{jj} -in” category (where the two leading jets in the event reconstruct the W mass, $m_{jj} \sim m_W$) are the most sensitive of the two-lepton same-sign ($2\ell^{\text{SS}}$) categories (see auxiliary Fig. 24 of Ref. [27]), and we concentrate on those here to obtain a conservative limit. The relevant CMS analysis cuts for the $2\ell^{\text{SS}}$ in this category are

$$\begin{aligned} p_T^{\ell_{1,2}} &> 25 \text{ GeV}, \quad m_{\ell\ell} > 20 \text{ GeV}, \quad m_{jj} \in [65, 95] \text{ GeV} \text{ (“}m_{jj} \text{ in”)}, \\ E_T^{\text{miss}} &> 45 \text{ GeV}, \quad m_T^{\text{max}}(\ell) > 90 \text{ GeV}, \end{aligned} \quad (3.2)$$

with ℓ_1 and ℓ_2 the leading and subleading leptons in p_T , and $m_T^{\text{max}}(\ell)$ defined as the transverse mass built from the missing transverse energy E_T^{miss} and the hardest lepton. The cut efficiencies for the BSM (ϵ_S) and the SM (ϵ_B) triboson signals are

$$\epsilon_S = 0.45 \quad , \quad \epsilon_B = 0.27. \quad (3.3)$$

Note that the CMS analysis is designed to extract the SM triboson signal from the SM background, hence the relatively high ϵ_B here. The SM background and observed SM signal

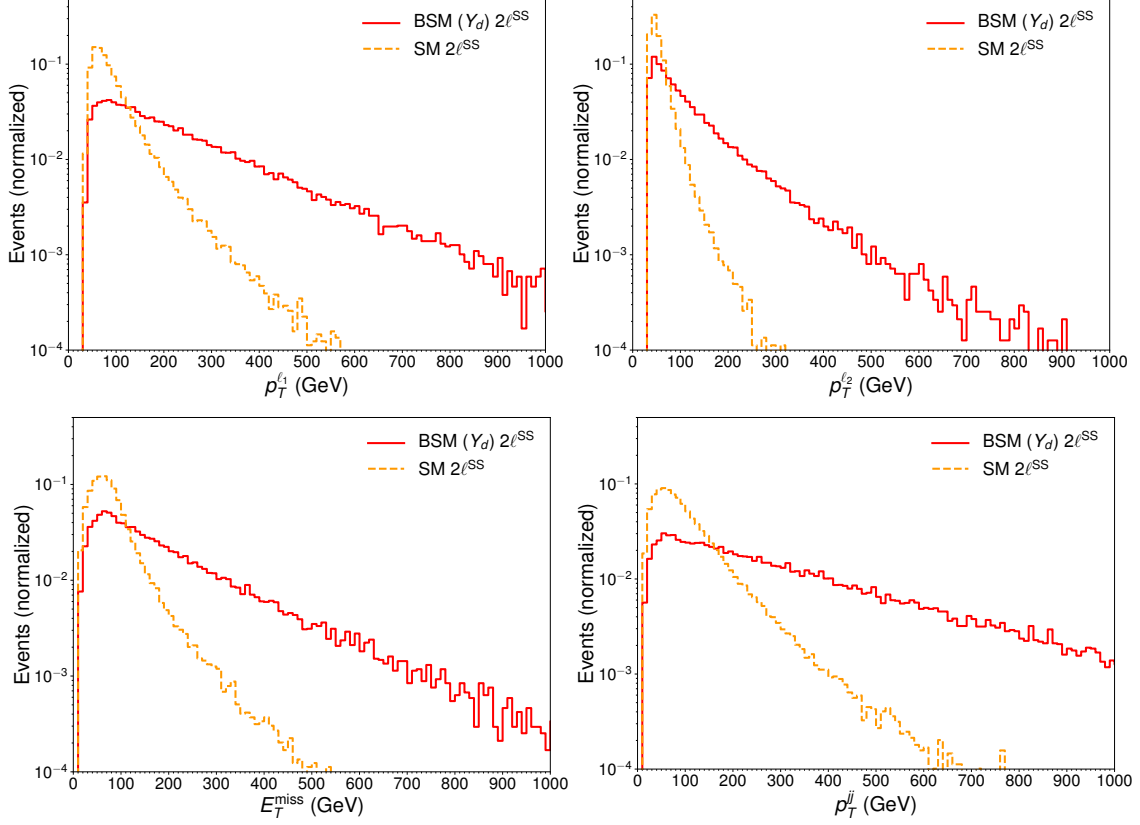


Figure 3. Normalized (to unit area) WW same-sign di-lepton channel differential distributions for $p_T^{\ell_1}$ (top-left), $p_T^{\ell_2}$ (top-right), E_T^{miss} (bottom-left) and p_T^{jj} (bottom-right), for the pure Y_d BSM triboson signal (solid-red lines) and the SM triboson contribution (dashed-yellow lines) at the 14 TeV LHC.

events for the cut-based CMS “ m_{jj} -in” $\mu^\pm\mu^\pm$ and $e^\pm\mu^\pm$ selection categories are given in the auxiliary Table 5 of Ref. [27]. For the $e^\pm\mu^\pm$ category, the expected SM background, expected SM WW signal and the observed number of events are, respectively, 35.2, 3.3 and 46. For the $\mu^\pm\mu^\pm$ category these numbers are 24.6, 3.5 and 20.

By computing the expected ratio of BSM to SM triboson events as a function of Y_d from (3.2) and (3.3) and normalizing to the CMS expected number of SM triboson events in each signal region, we obtain a 2σ bound⁴

$$\delta y_d \lesssim 6800 \quad (\text{LHC CMS analysis [27]}). \quad (3.4)$$

It is clear that the current $2\ell^{\text{SS}}$ CMS analysis is not tailored to search for deviations in the light-quark Yukawa couplings from their SM values. Large improvements in the sensitivity to δy_q can be obtained by a more stringent event selection, as illustrated in Fig. 3 for the normalized $p_T^{\ell_1}$, $p_T^{\ell_2}$, E_T^{miss} and p_T^{jj} (transverse momentum of the leading di-jet system) distributions for BSM and SM triboson $2\ell^{\text{SS}}$ signal at the $\sqrt{s} = 14$ TeV LHC. To illustrate this large potential improvement, we apply the following set of cuts for a $2\ell^{\text{SS}}$

⁴Here and in all of the following, the bounds implicitly refer to the magnitude of δy_q , that is $\delta y_q \equiv |\delta y_q|$.

triboson analysis at the HL-LHC,

$$p_T^{\ell_{1,2}} > 60 \text{ GeV} , \quad E_T^{\text{miss}} > 120 \text{ GeV} , \quad p_T^{jj} > 120 \text{ GeV} , \quad |\Delta\eta(\ell_1, \ell_2)| < 2 , \quad (3.5)$$

where the two jets (jj) come from the reconstructed hadronically-decayed W . For an analysis at the FCC-hh, the harder kinematics for the BSM triboson signal as compared to the LHC allows for even tighter cuts,

$$p_T^{\ell_{1,2}} > 100 \text{ GeV} , \quad E_T^{\text{miss}} > 150 \text{ GeV} , \quad p_T^{jj} > 150 \text{ GeV} , \quad |\Delta\eta(\ell_1, \ell_2)| < 2 . \quad (3.6)$$

The leptons are considered within the pseudorapidity acceptance $|\eta| < 2.5$. A veto on a third lepton with $p_T > 10 \text{ GeV}$ is applied. We find the following efficiencies for the δy_d BSM (ϵ_S) and SM (ϵ_B) triboson processes,

$$\begin{aligned} \epsilon_S &= 0.61 \text{ (HL-LHC)} \quad , \quad \epsilon_S = 0.61 \text{ (FCC-hh)} , \\ \epsilon_B &= 0.015 \text{ (HL-LHC)} \quad , \quad \epsilon_B = 0.0055 \text{ (FCC-hh)} . \end{aligned} \quad (3.7)$$

This analysis can be repeated for a BSM contribution with $\delta y_u \neq 0$ (same efficiencies as for $\delta y_d \neq 0$) or $\delta y_s \neq 0$, and for the case of a strange Yukawa modification we obtain an efficiency $\epsilon_S^s = 0.48$ at the HL-LHC and $\epsilon_S^s = 0.4$ at the FCC-hh with the cuts (3.5) and (3.6), respectively. We assume throughout a luminosity of $2 \times 3 \text{ ab}^{-1} = 6 \text{ ab}^{-1}$ for ATLAS and CMS combined at the HL-LHC and $2 \times 15 \text{ ab}^{-1} = 30 \text{ ab}^{-1}$ at FCC-hh.

In the limit of negligible reducible SM background (which we estimate below) to the $2\ell^{\text{SS}}$ triboson search, the estimated 2σ bounds on the Higgs Yukawa couplings to light quarks from the above event selection are

$$\begin{aligned} \delta y_d &\lesssim 550 \text{ (HL-LHC)} \quad , \quad \lesssim 63 \text{ (FCC-hh)} , \\ \delta y_u &\lesssim 1100 \text{ (HL-LHC)} \quad , \quad \lesssim 130 \text{ (FCC-hh)} , \\ \delta y_s &\lesssim 150 \text{ (HL-LHC)} \quad , \quad \lesssim 15 \text{ (FCC-hh)} . \end{aligned} \quad (3.8)$$

We now estimate the effect of the reducible SM backgrounds. We compute the dominant contributions, identified as the production of a $t\bar{t}$ pair in association with a weak boson ($t\bar{t}W^\pm$, $t\bar{t}Z$), as well as the process $pp \rightarrow W^\pm Z jj$ with one of the leptons from the weak boson decays falling out of the detector acceptance. We estimate these processes at NLO in QCD for $t\bar{t}V$ ($V = W^\pm, Z$) and LO for Zjj . A b -tagging performance similar to the CMS DeepCSV b -tagging algorithm [44] is assumed for both HL-LHC and FCC-hh cases. A veto on the presence of b -jets can be applied to reject a large fraction of the $t\bar{t}W^\pm$ and $t\bar{t}Z$ events (the corresponding veto efficiency on the BSM signal is neglected). The sum of $t\bar{t}W^\pm$ and $t\bar{t}Z$ reducible SM backgrounds then account for an event yield equal to 5% (21%) of the irreducible SM background at the HL-LHC (FCC-hh), while the $W^\pm Z jj$ SM background accounts for 14% (47%). When including the reducible background, the Higgs Yukawa coupling bounds become:

$$\begin{aligned} \delta y_d &\lesssim 570 \text{ (HL-LHC)} \quad , \quad \lesssim 71 \text{ (FCC-hh)} , \\ \delta y_u &\lesssim 1200 \text{ (HL-LHC)} \quad , \quad \lesssim 150 \text{ (FCC-hh)} , \\ \delta y_s &\lesssim 160 \text{ (HL-LHC)} \quad , \quad \lesssim 17 \text{ (FCC-hh)} , \end{aligned} \quad (3.9)$$

which shows only a very small degradation in sensitivity with respect to (3.8).

Finally, the sensitivity can be improved by performing shape analyses of relevant kinematic distributions, as those shown in Fig. 3, which can exploit the different kinematic behaviour of BSM signal compared to the SM. In our study we will consider the p_T distribution of the leading lepton, though we note that further improvement of the sensitivity can be obtained by a comprehensive analysis of multiple distributions. We adopt the following binned log-likelihood:

$$\Lambda(\delta y_q) = -2 \sum_i^{\text{bins}} \log \frac{L(S_i + B_i, B_i)}{L(B_i, B_i)} \quad (3.10)$$

where $L(\lambda, k)$ is the Poisson distribution with mean λ and occurrence k in each bin, and $S_i(B_i)$ is the expected signal (background) yield in i^{th} bin. We use the following binning for the HL-LHC: bins of 10 GeV from 60 GeV to 600 GeV, 50 GeV from 600 GeV to 1 TeV, and an overflow bin for all events above 1 TeV. For the FCC we use bins of 50 GeV from 100 GeV to 1.6 TeV, 100 GeV until 2.4 TeV, and an overflow bin for all events above 2.4 TeV. The resulting expected sensitivities for $\Lambda(\delta y_q) = 4$ are found to be

$$\begin{aligned} \delta y_d &\lesssim 430 \text{ (HL-LHC)} \quad , \quad \lesssim 36 \text{ (FCC-hh)}, \\ \delta y_u &\lesssim 850 \text{ (HL-LHC)} \quad , \quad \lesssim 71 \text{ (FCC-hh)}, \\ \delta y_s &\lesssim 150 \text{ (HL-LHC)} \quad , \quad \lesssim 13 \text{ (FCC-hh)}. \end{aligned} \quad (3.11)$$

This is the improvement one can expect over the cut and count estimate in Eq. (3.8) by using the differential information of the lepton p_T .

3.2 WWW: three-lepton final state

We now analyse the three-lepton channel $pp \rightarrow W^\pm W^\pm W^\mp \rightarrow \ell^\pm \ell^\pm \ell^\mp \nu\nu\nu$. The normalized differential distributions for the leading and subleading lepton transverse momenta $p_T^{\ell_{1,2}}$, the missing transverse energy E_T^{miss} and the angular separation between the same-sign leptons in the transverse plane $|\Delta\Phi(\ell^\pm, \ell^\pm)|$ of the BSM triboson signal and the SM triboson background are shown in Fig. 4 for the $\sqrt{s} = 14$ TeV HL-LHC and the FCC-hh. Applying the following selection cuts for the HL-LHC,

$$p_T^{\ell_1} > 70 \text{ GeV}, \quad p_T^{\ell_2} > 50 \text{ GeV}, \quad p_T^{\ell_3} > 30 \text{ GeV}, \quad E_T^{\text{miss}} > 80 \text{ GeV}, \quad |\Delta\Phi(\ell^\pm, \ell^\pm)| > 2, \quad (3.12)$$

and a tighter set of cuts for the FCC-hh

$$p_T^{\ell_1} > 150 \text{ GeV}, \quad p_T^{\ell_2} > 80 \text{ GeV}, \quad p_T^{\ell_3} > 50 \text{ GeV}, \quad E_T^{\text{miss}} > 120 \text{ GeV}, \quad |\Delta\Phi(\ell^\pm, \ell^\pm)| > 1.5, \quad (3.13)$$

we find the following efficiencies for the δy_u and δy_d BSM signal (ϵ_S) and the SM (ϵ_B) triboson processes,

$$\begin{aligned} \epsilon_S &= 0.62 \text{ (HL-LHC)} \quad , \quad \epsilon_S = 0.50 \text{ (FCC-hh)}, \\ \epsilon_B &= 0.037 \text{ (HL-LHC)} \quad , \quad \epsilon_B = 0.014 \text{ (FCC-hh)}. \end{aligned} \quad (3.14)$$

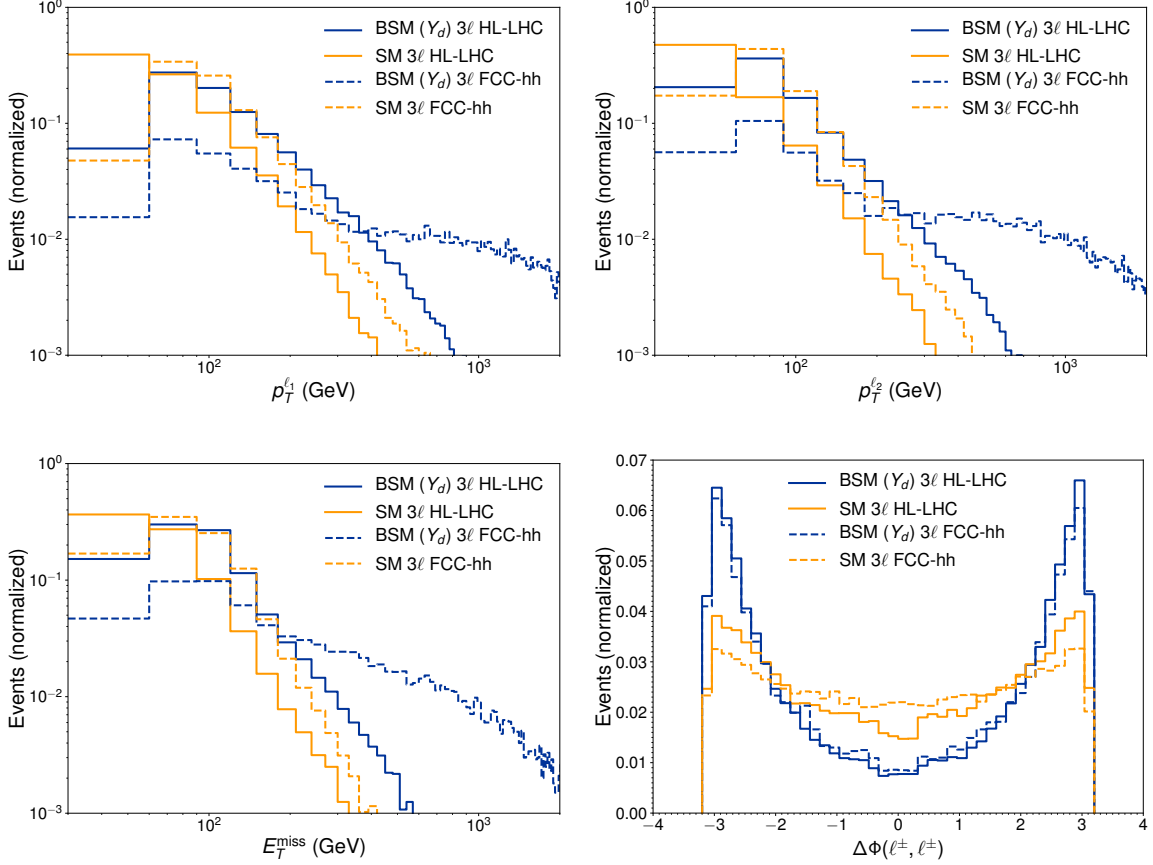


Figure 4. Normalized (to unit area) WWW tri-lepton channel differential distributions for $p_T^{\ell_1}$ (top-left), $p_T^{\ell_2}$ (top-right), E_T^{miss} (bottom-left) and $\Delta\Phi(\ell^\pm, \ell^\pm)$ (bottom-right), for the pure Y_d BSM triboson signal (blue lines) and the SM triboson contribution (yellow lines) at the 14 TeV LHC (solid) and 100 TeV FCC (dashed).

For the BSM signal with $\delta y_s \neq 0$, the respective signal efficiencies are $\epsilon_S^s = 0.6$ at the HL-LHC and $\epsilon_S^s = 0.16$ at the FCC-hh.

In the limit of negligible reducible background, the estimated 2σ bounds on δy_q are

$$\begin{aligned}
 \delta y_d &\lesssim 900 \text{ (HL-LHC)} \quad , \quad \lesssim 120 \text{ (FCC-hh)} \quad , \\
 \delta y_u &\lesssim 1900 \text{ (HL-LHC)} \quad , \quad \lesssim 240 \text{ (FCC-hh)} \quad , \\
 \delta y_s &\lesssim 230 \text{ (HL-LHC)} \quad , \quad \lesssim 40 \text{ (FCC-hh)} \quad .
 \end{aligned}
 \tag{3.15}$$

The dominant reducible backgrounds consist on the production of a top pair in association with a heavy vector boson, with at least three leptons in the final state. We have computed the corresponding $t\bar{t}W^\pm$ and $t\bar{t}Z$ processes at NLO in QCD for HL-LHC and FCC-hh. Imposing a b -jet veto after the selections (3.12) and (3.13) reduces the combination of $t\bar{t}W^\pm$ and $t\bar{t}Z$ background contributions to a 5.2% of the irreducible background for HL-LHC and 3.6% of the irreducible background for FCC-hh. As such, the sensitivity estimates (3.15) do not change appreciably when the dominant reducible SM backgrounds

are included in the analysis. We also note that $ZW^\pm W^\mp$ and ZZW^\pm processes, which could in principle constitute reducible backgrounds for our $W^\pm W^\pm W^\mp$ tri-lepton search, can be made negligible by a fourth lepton veto in combination with a di-lepton Z -mass veto. Besides, for $\delta y_q \neq 0$ the $ZW^\pm W^\mp$ and ZZW^\pm processes could also be regarded as a BSM signal so it is conservative to omit them in our tri-lepton analysis.

As discussed in Section 3.1, performing a binned shape analysis may significantly improve the sensitivity with respect to the cut and count selection described above. For example, using the leading lepton p_T differential distribution, as shown in Fig. 4, gives the following 2σ projected bounds from the three-lepton channel alone:

$$\begin{aligned}\delta y_d &\lesssim 840 \text{ (HL-LHC)} \quad , \quad \lesssim 54 \text{ (FCC-hh)} \text{ ,} \\ \delta y_u &\lesssim 1700 \text{ (HL-LHC)} \quad , \quad \lesssim 110 \text{ (FCC-hh)} \text{ ,} \\ \delta y_s &\lesssim 230 \text{ (HL-LHC)} \quad , \quad \lesssim 33 \text{ (FCC-hh)} \text{ .}\end{aligned}\tag{3.16}$$

Here, we use the following binning for the HL-LHC: bins of 10 GeV from 70 GeV to 600 GeV, 50 GeV from 600 GeV to 900 GeV, and an overflow bin for all events above 900 GeV. For the FCC we use bins of 10 GeV from 150 GeV to 200 GeV, 50 GeV from 200 GeV to 1.5 TeV, 100 GeV from 1.5 TeV to 2.2 TeV, and an overflow bin for all events above 2.2 TeV.

Finally, we note that the total WWW sensitivity would benefit from combining its various decay channels. For example a combination of the shape analyses for the same-sign di-lepton and three-lepton channels, neglecting correlations, yields the improved bounds

$$\begin{aligned}\delta y_d &\lesssim 420 \text{ (HL-LHC)} \quad , \quad \lesssim 34 \text{ (FCC-hh)} \text{ ,} \\ \delta y_u &\lesssim 830 \text{ (HL-LHC)} \quad , \quad \lesssim 68 \text{ (FCC-hh)} \text{ ,} \\ \delta y_s &\lesssim 140 \text{ (HL-LHC)} \quad , \quad \lesssim 13 \text{ (FCC-hh)} \text{ .}\end{aligned}\tag{3.17}$$

These sensitivities are clearly dominated by the signal in the same-sign dilepton final state.

3.3 ZZZ : four-lepton final state

We move to discussing the sensitivity of the ZZZ channel to light Yukawas. As discussed previously, combining that with the sensitivity analyses of the WWW channel from Sections 3.1 and 3.2 in principle allows one to disentangle the effects of δy_u and δy_d . In addition, the cross section values of Table 2 indicate that ZZZ production could at the same time yield strong sensitivity to the presence of $\delta y_s \neq 0$.

Regarding possible ZZZ decay channels, we note that the 6ℓ final state, despite being the cleanest channel, suffers from too low a cross-section and thus it does not allow to obtain competitive limits. We then focus here on the 4ℓ final states: $pp \rightarrow ZZZ \rightarrow 4\ell + 2\nu$ and $pp \rightarrow ZZZ \rightarrow 4\ell + 2j$. In the following we shall perform a naive estimate of the sensitivity to δy_q in both channels.

3.3.1 $4\ell + E_T^{\text{miss}}$

The $4\ell + 2\nu$ decay channel of the ZZZ triboson process has the advantage of being easy to disentangle from the dominant reducible SM background, $pp \rightarrow ZZ \rightarrow 4\ell$, due to

the presence of E_T^{miss} from the neutrinos in the case of the signal. The two relevant irreducible SM backgrounds for our BSM process are the triboson processes ZZZ and WWZ . The latter becomes very suppressed by requiring two same-flavour lepton pairs reconstructing Z -masses, i.e. $|m_Z - m_{\ell\ell}| < 10$ GeV for each lepton pair. Similarly, the reducible SM backgrounds $t\bar{t}Z$, tWZ are suppressed to a negligible level by this requirement in combination with a b -jet veto [27]. For the ZZ reducible background, the inclusive cross section after the $Z \rightarrow \ell\ell$ decays is ~ 75 fb [45], much larger than that of the irreducible SM backgrounds. The presence of E_T^{miss} for $pp \rightarrow ZZ \rightarrow 4\ell$ is however due to detector resolution and potential mismeasurements, and thus it is expected to be very small above a certain E_T^{miss} range.

In the following, we consider events for which the following initial selection cuts are applied

$$p_T^{\ell_{1,2}} > 25 \text{ GeV}, p_T^{\ell_{3,4}} > 10 \text{ GeV}, |\eta_\ell| < 2.5, \Delta R_{\ell\ell} > 0.1, |m_Z - m_{\ell\ell}| < 10 \text{ GeV}. \quad (3.18)$$

The $pp \rightarrow ZZZ \rightarrow 4\ell + 2\nu$ cross section computed at LO for $\sqrt{s} = 14$ TeV LHC with these selection cuts is given by

$$\begin{aligned} \sigma(Y_u) &= 0.013 \text{ fb} + Y_u^2 \times 3.0 \text{ fb}, \\ \sigma(Y_d) &= 0.013 \text{ fb} + Y_d^2 \times 1.8 \text{ fb}, \\ \sigma(Y_s) &= 0.013 \text{ fb} + Y_s^2 \times 0.14 \text{ fb}, \end{aligned} \quad (3.19)$$

respectively for $\delta y_u \neq 0$, $\delta y_d \neq 0$ and $\delta y_s \neq 0$. In Fig. 5 (top) we show the normalized $p_T^{\ell_1}$ and E_T^{miss} distributions for the BSM signal and SM triboson ZZZ background, for the LHC with $\sqrt{s} = 14$ TeV. We also include in the plot for comparison the expected E_T^{miss} distribution for the ZZ reducible SM background after the selection (3.18) for $\sqrt{s} = 13$ TeV LHC, as given in [43] (and then normalized). This distribution can be accurately fitted by an exponentially decreasing function for $E_T^{\text{miss}} \gtrsim 50$ GeV. Thus, an E_T^{miss} cut greatly suppresses the ZZ reducible background, enhancing at the same time the sensitivity to δy_d with respect to the one obtained directly from (3.19). For the HL-LHC sensitivity estimate we select events with $E_T^{\text{miss}} > 200$ GeV. This selection yields a BSM signal efficiency $\epsilon_S = 0.74$ for $\delta y_d \neq 0$, and a SM ZZZ triboson background efficiency $\epsilon_B = 0.09$. For $\delta y_s \neq 0$, the BSM signal efficiency is $\epsilon_S = 0.64$. We also estimate the corresponding efficiency ϵ_{ZZ} for the reducible SM background via the exponential fit to the ZZ E_T^{miss} distribution, finding $\epsilon_{ZZ} \sim 1.3 \times 10^{-5}$, which renders it subdominant with respect to the irreducible ZZZ background.

For FCC-hh, the $pp \rightarrow ZZZ \rightarrow 4\ell + 2\nu$ cross section at LO reads

$$\begin{aligned} \sigma(Y_u) &= 0.11 \text{ fb} + Y_u^2 \times 340 \text{ fb}, \\ \sigma(Y_d) &= 0.11 \text{ fb} + Y_d^2 \times 220 \text{ fb}, \\ \sigma(Y_s) &= 0.11 \text{ fb} + Y_s^2 \times 26 \text{ fb}, \end{aligned} \quad (3.20)$$

with the same basic cuts as for the HL-LHC analysis except for the $\Delta R_{\ell\ell}$ cut, which we set to $\Delta R_{\ell\ell} > 0.01$. The normalized distributions for $p_T^{\ell_1}$ and E_T^{miss} in this case are shown in Fig. 5 (bottom). For FCC-hh we set the signal selection cut $E_T^{\text{miss}} > 500$ GeV.

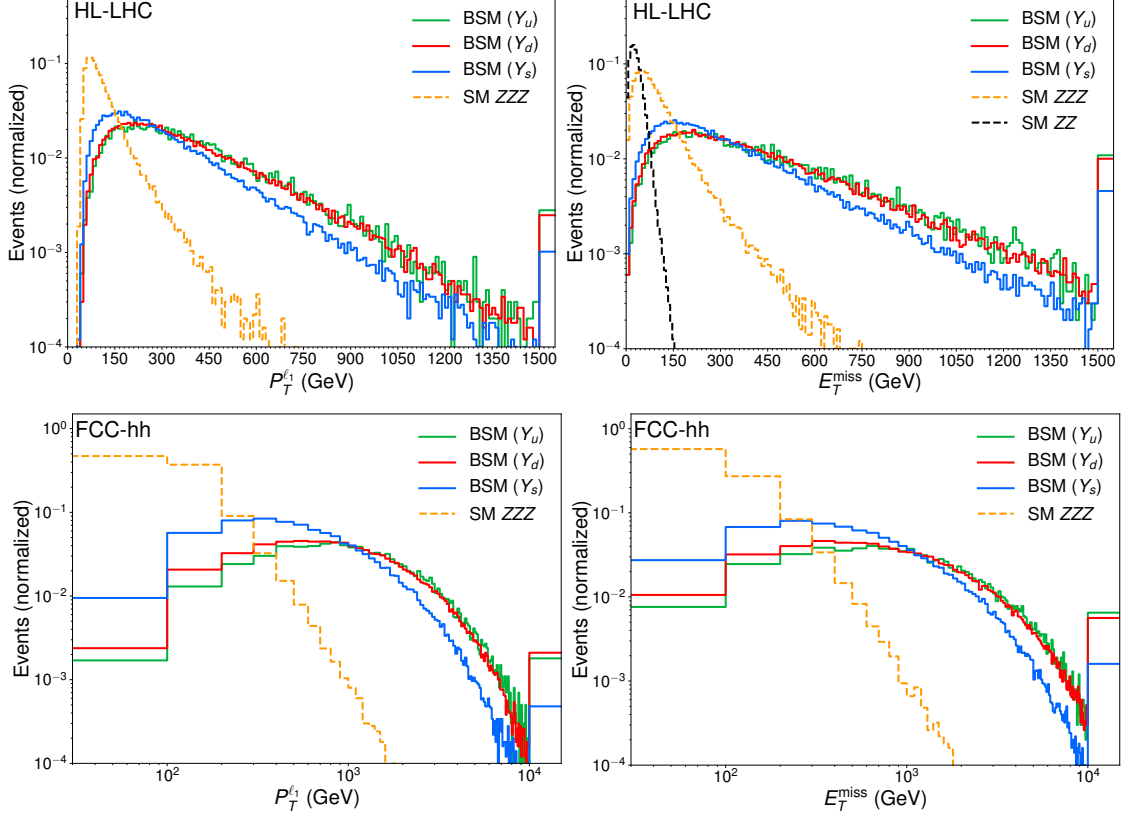


Figure 5. Normalized (to unit area) $pp \rightarrow ZZZ \rightarrow 4\ell + 2\nu$ differential distributions for $p_T^{\ell_1}$ (left) and E_T^{miss} (right) for the pure Y_d BSM triboson signal (solid-red), pure Y_u BSM triboson signal (solid-), pure Y_s BSM triboson signal (solid-blue), and the SM triboson contribution (dashed-yellow) at the 14 TeV LHC (top) and 100 TeV FCC (bottom). For HL-LHC E_T^{miss} (top-right) we also include the ZZ reducible SM background as a dashed-black line (see text for details). In each plot, the last bin corresponds to the overflow bin.

In order to derive sensitivity projections, we use an NLO k -factor of $k = 1.28$ [18] for the BSM signal, both for LHC and FCC-hh. For the ZZZ background, to normalise to the NLO cross-sections of Table 2, we use $k = 1.55$ (1.67) for HL-LHC (FCC-hh). The resulting projected 2σ sensitivities after signal selection are found to be

$$\begin{aligned}
 \delta y_d &\lesssim 1700 \quad (\text{HL-LHC}) \quad , \quad \lesssim 120 \quad (\text{FCC-hh}) \quad , \\
 \delta y_u &\lesssim 2600 \quad (\text{HL-LHC}) \quad , \quad \lesssim 190 \quad (\text{FCC-hh}) \quad , \\
 \delta y_s &\lesssim 340 \quad (\text{HL-LHC}) \quad , \quad \lesssim 19 \quad (\text{FCC-hh}) \quad .
 \end{aligned}
 \tag{3.21}$$

Applying instead a shape analysis to the E_T^{miss} differential distribution via a binned log-likelihood, as described in Section 3.1, gives the projected sensitivities

$$\begin{aligned}
 \delta y_d &\lesssim 1500 \quad (\text{HL-LHC}) \quad , \quad \lesssim 65 \quad (\text{FCC-hh}) \quad , \\
 \delta y_u &\lesssim 2300 \quad (\text{HL-LHC}) \quad , \quad \lesssim 100 \quad (\text{FCC-hh}) \quad , \\
 \delta y_s &\lesssim 300 \quad (\text{HL-LHC}) \quad , \quad \lesssim 12 \quad (\text{FCC-hh}) \quad .
 \end{aligned}
 \tag{3.22}$$

We used the following binning of E_T^{miss} for the HL-LHC: bins of 10 GeV from 0 GeV to 800 GeV, 50 GeV from 800 GeV to 1 TeV, and an overflow bin for all events above 1 TeV. For the FCC-hh we use bins of 100 GeV from 0 GeV to 2 TeV, and an overflow bin for all events above 2 TeV.

3.3.2 $4\ell + 2j$

Finally we consider the ZZZ sub-channel in which one Z -boson decays hadronically, yielding a $4\ell + 2j$ final state. This benefits from more statistics, yet has less clean backgrounds than purely leptonic final states as studied in the previous section: the $4\ell + 2j$ final state has a factor ~ 3 higher cross section than the $4\ell + E_T^{\text{miss}}$ one, but is more difficult to disentangle from the dominant SM reducible background, ZZ . In fact, as opposed to the previous scenario, the dominant background in this case is given by the SM ZZ +jets production. This contribution is estimated at LO in QCD with two partons in the final state ($ZZjj$). In order to distinguish our BSM signal from this background, we first apply a minimal set of cuts, aimed at discarding the events where the two leading jets do not reconstruct a hadronically decaying Z -boson. We then exploit the kinematical properties of the BSM signal, which is characterized by harder final particles, by applying a cut on the leading lepton $p_T^{\ell_1} > 150$ GeV (300 GeV) for HL-LHC (FCC-hh). The set of cuts we apply is

$$p_T^{\ell_1} > 150 \text{ (300) GeV}, p_T^{\ell_{2,3,4}} > 25 \text{ GeV}, p_T^j > 30 \text{ GeV}, M_{jj} \in [81, 101] \text{ GeV}, \quad (3.23)$$

where M_{jj} denotes the invariant mass of the two leading jets. The resulting 2σ projected bounds for our cut and count analysis are

$$\begin{aligned} \delta y_d &\lesssim 1800 \text{ (HL-LHC)} \quad , \quad \lesssim 170 \text{ (FCC-hh)}, \\ \delta y_u &\lesssim 2700 \text{ (HL-LHC)} \quad , \quad \lesssim 260 \text{ (FCC-hh)}, \\ \delta y_s &\lesssim 380 \text{ (HL-LHC)} \quad , \quad \lesssim 27 \text{ (FCC-hh)}. \end{aligned} \quad (3.24)$$

Performing a shape analysis on the leading lepton p_T distribution, as described in Section 3.1, gives the improved limits

$$\begin{aligned} \delta y_d &\lesssim 1300 \text{ (HL-LHC)} \quad , \quad \lesssim 93 \text{ (FCC-hh)}, \\ \delta y_u &\lesssim 1800 \text{ (HL-LHC)} \quad , \quad \lesssim 140 \text{ (FCC-hh)}, \\ \delta y_s &\lesssim 290 \text{ (HL-LHC)} \quad , \quad \lesssim 16 \text{ (FCC-hh)}. \end{aligned} \quad (3.25)$$

Here, we use the following binning of p_T^ℓ for both the HL-LHC and FCC: bins of 10 GeV from 40 GeV to 300 GeV, 50 GeV from 300 GeV to 600 GeV, and an overflow bin for all events above 600 GeV.

Since the two ZZZ channels, $4\ell + E_T^{\text{miss}}$ and $4\ell + 2j$, provide similar sensitivities in Eqs. (3.22) and (3.25), a combination of the shape analyses for the two channels, neglecting correlations, improves the sensitivity of the ZZZ triboson process,

$$\begin{aligned} \delta y_d &\lesssim 1100 \text{ (HL-LHC)} \quad , \quad \lesssim 60 \text{ (FCC-hh)}, \\ \delta y_u &\lesssim 1600 \text{ (HL-LHC)} \quad , \quad \lesssim 92 \text{ (FCC-hh)}, \\ \delta y_s &\lesssim 250 \text{ (HL-LHC)} \quad , \quad \lesssim 11 \text{ (FCC-hh)}. \end{aligned} \quad (3.26)$$

By comparing these results with those in Sections 3.1 and 3.2, we see that the WWW 2ℓ same-sign and 3ℓ analyses are more sensitive in general due to their higher statistics. Indeed, for $\delta y_d \neq 0$ the cross section for $pp \rightarrow W^\pm W^\pm W^\mp \rightarrow \ell^\pm \ell^\pm + 2\nu + 2j$ is approximately 100 times larger than that of $pp \rightarrow ZZZ \rightarrow 4\ell + 2\nu$. Yet, due to the larger cross section enhancement from LHC to FCC-hh in the case of ZZZ with respect to WWW (see Table 2), the sensitivity to $\delta y_q \neq 0$ in ZZZ channels at FCC-hh becomes competitive with that of WWW , particularly for the strange Yukawa coupling.

4 Comparison with other constraints

The sensitivity of the triboson analysis established in the previous Sections should be compared to the sensitivity of other existing probes of the light quark Yukawa couplings.

A change in the Higgs decay width into light quarks has an indirect effect on the event rate in other decay channels measured by the LHC collaborations. In particular, assuming only one Yukawa coupling is modified at a time, the total Higgs signal strength normalized to the SM value is given by the expression

$$\mu = \frac{1}{1 + \sum_q (2\delta y_q + \delta y_q^2) \text{Br}(h \rightarrow qq)_{\text{SM}}}. \quad (4.1)$$

The above holds when the total Higgs production cross section is not significantly affected by the enhanced $q\bar{q} \rightarrow h$ $qg \rightarrow qh$ modes, which is a good approximation for $\delta y_u \lesssim 1000$, $\delta y_d \lesssim 500$. Given the $\text{Br}(h \rightarrow qq)_{\text{SM}}$ in Table 1, for $q = u, d, s$ the effect is observable only for $|\delta y_q| \gg 1$, and then the linear term in δy_q in Eq. (4.1) is subleading compared to the quadratic one. Note that in this regime the Higgs signal strength is always *suppressed*, $\mu < 1$. The HL-LHC is expected to measure the total Higgs signal strength with an error of order 2-3% [46]. A future measurement $\mu = 1.00 \pm 0.03$ would set the following bounds on the Yukawa couplings:⁵

$$\delta y_d \lesssim 340, \quad \delta y_u \lesssim 700, \quad \delta y_s \lesssim 17 \quad (\text{HL-LHC}). \quad (4.2)$$

If the effect of the enhanced $q\bar{q} \rightarrow h$ is taken into account, the first two limits are slightly relaxed: $\delta y_d \lesssim 360$, $\delta y_u \lesssim 780$. Using the most recent measurements from CMS ($\mu = 1.02_{-0.06}^{+0.07}$ [2]) and ATLAS ($\mu = 1.06 \pm 0.07$ [1]) one finds the present bounds are already close to the HL-LHC expected ones:

$$\begin{aligned} \text{ATLAS : } & \delta y_d < 400, \quad \delta y_u < 820, \quad \delta y_s < 19, \\ \text{CMS : } & \delta y_d < 450, \quad \delta y_u < 930, \quad \delta y_s < 22, \end{aligned} \quad (4.3)$$

thanks to the small measured upward fluctuation of the Higgs signal strength in ATLAS. We consider very encouraging the fact that the sensitivity of the triboson analysis to the first generation Yukawas, cf. Table 3, is comparable to that in Eq. (4.2). Moreover, many new physics effects may affect the total Higgs signal strength, and cancellations

⁵As before, the left-hand-sides of all the δy_q bounds should be read as $|\delta y_q|$, but we omit the absolute value sign to simplify the notation.

between them are possible. Including the triboson input in the global Higgs fits will allow to lift degeneracies in the parameter space and obtain more robust constraints on the Higgs couplings. We also note that it will be challenging to significantly improve the sensitivity displayed in Eq. (4.2) at the LHC or future hadron colliders, due to QCD and PDF uncertainties affecting the SM theoretical prediction of the Higgs signal strength. This is in contrast with the sensitivity of the triboson analysis, which can be significantly improved by upgrading to FCC-hh. On the other hand, the sensitivity of the HL-LHC triboson analyses to the strange Yukawa is an $\mathcal{O}(10)$ factor weaker than the one in Eq. (4.2). Other theoretical ideas (or the FCC-hh) are needed to have a realistic chance of observing effects of enhanced y_s .

We may also compare the triboson sensitivity to δy_u and δy_d to those projected in other theoretical analyses in the literature, besides that of Higgs signal strength measurements. Enhanced light quark Yukawa couplings lead to a distortion of the p_T and rapidity distributions of the $pp \rightarrow h$ cross section with respect to the SM predictions due to a larger relative contribution of the $q\bar{q} \rightarrow h$ and $qg \rightarrow qh$ processes. Assuming the SM predictions can be controlled at the required level of accuracy, this can be explored at the HL-LHC to set the bounds $\delta y_d \lesssim 380$, $\delta y_u \lesssim 640$ [14] (see also [15, 17]), which are comparable to the triboson ones, yet depend on a different set of assumptions. In the SMEFT, the operators in Eq. (2.1) that lead to modified Higgs Yukawa couplings also generate analogous vertices with two (and three) Higgs bosons. Therefore one can constrain Yukawa couplings via Higgs pair production, leading to $\delta y_d \lesssim 850$, $\delta y_u \lesssim 1200$ [18] at the HL-LHC. Precision measurements of the charge asymmetry of the $W^\pm h$ associated production could lead to the HL-LHC bounds $\delta y_d \lesssim 1300$, $\delta y_u \lesssim 2900$ [16]. A large y_u would also enhance $q\bar{q}$ -initiated contributions to the $pp \rightarrow h\gamma$ process, from which the bound $\delta y_u \lesssim 2100$ could be set at the HL-LHC [19]. Finally, the exclusive Higgs decays $h \rightarrow \rho\gamma$ currently probe $\delta y_{u,d}$ of order 10^6 [11, 23], far from the rest of proposed light quark Yukawa probes. We remark that a synergy of several different probes of light Yukawa couplings will be crucial for lifting the various degeneracies in the vast parameter space of the SMEFT.

5 Conclusion

	WWW			ZZZ		
	$\ell^\pm \ell^\pm + 2\nu + 2j$	$\ell^\pm \ell^\pm \ell^\mp + 3\nu$	Comb.	$4\ell + 2\nu$	$4\ell + 2j$	Comb.
δy_d	430 (36)	840 (54)	420 (34)	1500 (65)	1300 (93)	1100 (60)
δy_u	850 (71)	1700 (110)	830 (68)	2300 (100)	1800 (140)	1600 (92)
δy_s	150 (13)	230 (33)	140 (13)	300 (12)	290 (16)	250 (11)

Table 3. Summary of the projected 2σ sensitivity to δy_q at the HL-LHC (FCC-hh) for the sub-channels considered in this study.

In this study we considered the sensitivity of triboson production to modifications of the up, down and strange Yukawa couplings. Unlike previously suggested probes that rely on on-shell Higgs decays, our proposal makes use of energy growth due to modifications of

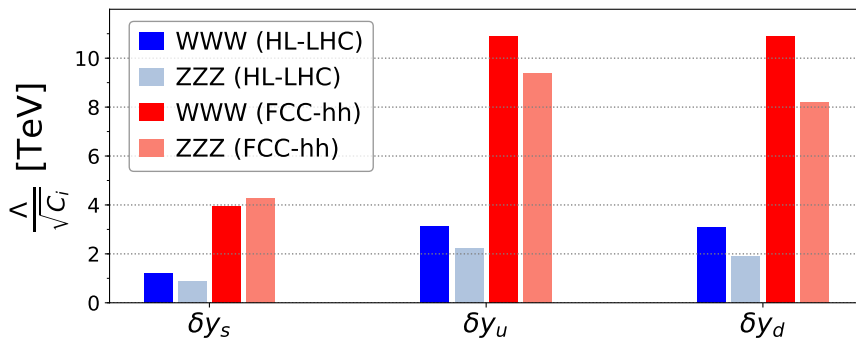


Figure 6. Projected 2σ reach at the HL-LHC (blue) and FCC-hh (red) on the dimension-6 operator scale Λ with Wilson coefficient C_i for the up, down, and strange Yukawa operators in (2.1). The darker shades are for the combination of the $pp \rightarrow WWW \rightarrow \ell^\pm \ell^\pm + 2\nu + 2j$ and $pp \rightarrow WWW \rightarrow \ell^\pm \ell^\pm \ell^\mp + 3\nu$ channels and lighter shades denote the combination of $pp \rightarrow ZZZ \rightarrow 4l + E_T^{\text{miss}}$ and $pp \rightarrow ZZZ \rightarrow 4l + 2j$.

the off-shell Higgs couplings. We showed that the current CMS triboson analysis constrains $\delta y \lesssim \mathcal{O}(1000)$ at 2σ but that this can be improved by an order of magnitude with more targeted cuts to $\delta y \lesssim \mathcal{O}(100)$ at HL-LHC, and, furthermore, to $\delta y \lesssim \mathcal{O}(10)$ at a future 100 TeV collider such as FCC-hh. A summary of the projected bounds are given in Table 3. The corresponding dimension-6 operator scales $\Lambda/\sqrt{C_i}$, defined from (2.1) as $Y_i = C_i v^2/\Lambda^2$ with Wilson coefficient C_i , are shown in Fig. 6 for the combination of the two WWW sub-channels and the two ZZZ channels. The former are the most sensitive at the HL-LHC, though we note that the ZZZ channel’s sensitivity will become comparable at FCC-hh. While these constraints are at the individual level, switching on one operator at a time while setting the others to zero, they can give an indication of the sensitivity of the measurements. In future work, the effects of other SMEFT operators could also be taken into account in a more general analysis, as well as NLO corrections to the differential distributions.

The experimentally allowed ranges of the light Yukawas are still unconstrained by several orders of magnitude. This can affect other observables (see e.g. Ref. [47]) and introduce degeneracies in global fits. Moreover, our lack of understanding of the pattern of Higgs couplings motivates probing even unnaturally large enhancements in the light Yukawas that may be difficult to obtain without tuning (see Refs. [47–51] for some examples of specific models). It is therefore important to reduce the experimental uncertainty as much as possible in the future. The study proposed here can be further refined, including more channels and combining related processes, in order to maximise the experimental information available and widen our window onto the mysterious Higgs sector.

Acknowledgments

We thank Elena Venturini for related collaboration and discussions, the organisers of the Les Houches workshop for the stimulating environment where this project was initiated, Hannsjörg Weber for correspondence regarding the CMS analysis and Francesco Riva for

correspondence regarding [26]. Feynman diagrams were drawn using TIKZ-FEYNMAN [52]. KT is supported by the US Department of Energy grant DE-SC0010102. TY is supported by a Branco Weiss Society in Science Fellowship and partially supported by STFC consolidated grant ST/P000681/1. NV is supported by the ERC grant NEO-NAT. AF is partially supported by the Agence Nationale de la Recherche (ANR) under grant ANR-19-CE31-0012 (project MORA). JMN was supported by Ramón y Cajal Fellowship contract RYC-2017-22986, and also acknowledges support from the Spanish MINECO’s “Centro de Excelencia Severo Ochoa” Programme under grant SEV-2016-0597, from the European Union’s Horizon 2020 research and innovation programme under the Marie Skłodowska-Curie grant agreement 860881 (ITN HIDDEN) and from the Spanish Proyectos de I+D de Generación de Conocimiento via grant PGC2018-096646-A-I00.

References

- [1] **ATLAS** Collaboration, *A combination of measurements of Higgs boson production and decay using up to 139 fb⁻¹ of proton–proton collision data at $\sqrt{s} = 13$ TeV collected with the ATLAS experiment*, *ATLAS-CONF-2020-027* (2020).
- [2] **CMS** Collaboration, *Combined Higgs boson production and decay measurements with up to 137 fb⁻¹ of proton-proton collision data at $\sqrt{s} = 13$ TeV*, *CMS-PAS-HIG-19-005* (2020).
- [3] **ATLAS** Collaboration, G. Aad et al., *A search for the dimuon decay of the Standard Model Higgs boson with the ATLAS detector*, [arXiv:2007.07830](https://arxiv.org/abs/2007.07830).
- [4] **CMS** Collaboration, A. M. Sirunyan et al., *Evidence for Higgs boson decay to a pair of muons*, [arXiv:2009.04363](https://arxiv.org/abs/2009.04363).
- [5] G. T. Bodwin, F. Petriello, S. Stoynev, and M. Velasco, *Higgs boson decays to quarkonia and the $H\bar{c}c$ coupling*, *Phys. Rev. D* **88** (2013), no. 5 053003, [[arXiv:1306.5770](https://arxiv.org/abs/1306.5770)].
- [6] G. Perez, Y. Soreq, E. Stamou, and K. Tobioka, *Constraining the charm Yukawa and Higgs-quark coupling universality*, *Phys. Rev. D* **92** (2015), no. 3 033016, [[arXiv:1503.00290](https://arxiv.org/abs/1503.00290)].
- [7] G. Perez, Y. Soreq, E. Stamou, and K. Tobioka, *Prospects for measuring the Higgs boson coupling to light quarks*, *Phys. Rev. D* **93** (2016), no. 1 013001, [[arXiv:1505.06689](https://arxiv.org/abs/1505.06689)].
- [8] I. Brivio, F. Goertz, and G. Isidori, *Probing the Charm Quark Yukawa Coupling in Higgs+Charm Production*, *Phys. Rev. Lett.* **115** (2015), no. 21 211801, [[arXiv:1507.02916](https://arxiv.org/abs/1507.02916)].
- [9] S. Mao, Y. Guo-He, L. Gang, Z. Yu, and G. Jian-You, *Probing the charm-Higgs Yukawa coupling via Higgs boson decay to h_c plus a photon*, *J. Phys. G* **46** (2019), no. 10 105008, [[arXiv:1905.01589](https://arxiv.org/abs/1905.01589)].
- [10] N. M. Coyle, C. E. M. Wagner, and V. Wei, *Bounding the charm Yukawa coupling*, *Phys. Rev.* **D100** (2019), no. 7 073013, [[arXiv:1905.09360](https://arxiv.org/abs/1905.09360)].
- [11] A. L. Kagan, G. Perez, F. Petriello, Y. Soreq, S. Stoynev, and J. Zupan, *Exclusive Window onto Higgs Yukawa Couplings*, *Phys. Rev. Lett.* **114** (2015), no. 10 101802, [[arXiv:1406.1722](https://arxiv.org/abs/1406.1722)].
- [12] M. König and M. Neubert, *Exclusive Radiative Higgs Decays as Probes of Light-Quark Yukawa Couplings*, *JHEP* **08** (2015) 012, [[arXiv:1505.03870](https://arxiv.org/abs/1505.03870)].

- [13] F. Bishara, U. Haisch, P. F. Monni, and E. Re, *Constraining Light-Quark Yukawa Couplings from Higgs Distributions*, *Phys. Rev. Lett.* **118** (2017), no. 12 121801, [[arXiv:1606.09253](#)].
- [14] Y. Soreq, H. X. Zhu, and J. Zupan, *Light quark Yukawa couplings from Higgs kinematics*, *JHEP* **12** (2016) 045, [[arXiv:1606.09621](#)].
- [15] G. Bonner and H. E. Logan, *Constraining the Higgs couplings to up and down quarks using production kinematics at the CERN Large Hadron Collider*, [arXiv:1608.04376](#).
- [16] F. Yu, *Phenomenology of Enhanced Light Quark Yukawa Couplings and the $W^{\pm}h$ Charge Asymmetry*, *JHEP* **02** (2017) 083, [[arXiv:1609.06592](#)].
- [17] J. Cohen, S. Bar-Shalom, G. Eilam, and A. Soni, *Light-quarks Yukawa couplings and new physics in exclusive high- p_T Higgs boson + jet and Higgs boson + b-jet events*, *Phys. Rev. D* **97** (2018), no. 5 055014, [[arXiv:1705.09295](#)].
- [18] L. Alasfar, R. Corral Lopez, and R. Gröber, *Probing Higgs couplings to light quarks via Higgs pair production*, *JHEP* **11** (2019) 088, [[arXiv:1909.05279](#)].
- [19] J. Aguilar-Saavedra, J. Cano, and J. No, *More light on Higgs flavor at the LHC: Higgs couplings to light quarks through $h + \gamma$ production*, [arXiv:2008.12538](#).
- [20] **ATLAS** Collaboration, G. Aad et al., *Search for Higgs and Z Boson Decays to $J/\psi \gamma$ and $\Upsilon(nS)\gamma$ with the ATLAS Detector*, *Phys. Rev. Lett.* **114** (2015), no. 12 121801, [[arXiv:1501.03276](#)].
- [21] **ATLAS** Collaboration, M. Aaboud et al., *Search for Higgs and Z Boson Decays to $\phi \gamma$ with the ATLAS Detector*, *Phys. Rev. Lett.* **117** (2016), no. 11 111802, [[arXiv:1607.03400](#)].
- [22] **LHCb** Collaboration, X. Cid Vidal et al., *Search for $H^0 \rightarrow b\bar{b}$ or $c\bar{c}$ in association with a W or Z boson in the forward region of pp collisions*, *LHCb-CONF-2016-006* (2016).
- [23] **ATLAS** Collaboration, M. Aaboud et al., *Search for exclusive Higgs and Z boson decays to $\phi \gamma$ and $\rho \gamma$ with the ATLAS detector*, *JHEP* **07** (2018) 127, [[arXiv:1712.02758](#)].
- [24] **ATLAS** Collaboration, M. Aaboud et al., *Search for the Decay of the Higgs Boson to Charm Quarks with the ATLAS Experiment*, *Phys. Rev. Lett.* **120** (2018), no. 21 211802, [[arXiv:1802.04329](#)].
- [25] **CMS** Collaboration, A. M. Sirunyan et al., *Search for decays of the 125 GeV Higgs boson into a Z boson and a ρ or ϕ meson*, *JHEP* **11** (2020) 039, [[arXiv:2007.05122](#)].
- [26] B. Henning, D. Lombardo, M. Riemann, and F. Riva, *Measuring Higgs Couplings without Higgs Bosons*, *Phys. Rev. Lett.* **123** (2019), no. 18 181801, [[arXiv:1812.09299](#)].
- [27] **CMS** Collaboration, *Observation of heavy triboson production in leptonic final states in proton-proton collisions at $\sqrt{s} = 13$ TeV*, *CMS-PAS-SMP-19-014* (2020).
- [28] **CMS** Collaboration, A. M. Sirunyan et al., *Observation of the production of three massive gauge bosons at $\sqrt{s} = 13$ TeV*, [arXiv:2006.11191](#).
- [29] B. W. Lee, C. Quigg, and H. Thacker, *Weak Interactions at Very High-Energies: The Role of the Higgs Boson Mass*, *Phys. Rev. D* **16** (1977) 1519.
- [30] G. Brooijmans et al., *Les Houches 2019 Physics at TeV Colliders: New Physics Working Group Report*, in *11th Les Houches Workshop on Physics at TeV Colliders: PhysTeV Les Houches*, 2, 2020. [arXiv:2002.12220](#).
- [31] F. Maltoni, L. Mantani, and K. Mimasu, *Modified interactions in the top-quark electroweak sector: exploiting unitarity violating effects at the amplitude level to probe New Physics*, in

- 2019 European Physical Society Conference on High Energy Physics, 10, 2019.
[arXiv:1910.05053](#).
- [32] C. Degrande, F. Maltoni, K. Mimasu, E. Vryonidou, and C. Zhang, *Single-top associated production with a Z or H boson at the LHC: the SMEFT interpretation*, *JHEP* **10** (2018) 005, [[arXiv:1804.07773](#)].
- [33] **Particle Data Group** Collaboration, M. Tanabashi et al., *Review of Particle Physics*, *Phys. Rev. D* **98** (2018), no. 3 030001.
- [34] **Flavour Lattice Averaging Group** Collaboration, S. Aoki et al., *FLAG Review 2019: Flavour Lattice Averaging Group (FLAG)*, *Eur. Phys. J. C* **80** (2020), no. 2 113, [[arXiv:1902.08191](#)].
- [35] K. Chetyrkin, *Quark mass anomalous dimension to $\mathcal{O}(\alpha_s^4)$* , *Phys. Lett. B* **404** (1997) 161–165, [[hep-ph/9703278](#)].
- [36] J. Vermaseren, S. Larin, and T. van Ritbergen, *The four loop quark mass anomalous dimension and the invariant quark mass*, *Phys. Lett. B* **405** (1997) 327–333, [[hep-ph/9703284](#)].
- [37] P. Baikov, K. Chetyrkin, and J. Kühn, *Five-Loop Running of the QCD coupling constant*, *Phys. Rev. Lett.* **118** (2017), no. 8 082002, [[arXiv:1606.08659](#)].
- [38] C. Englert and M. Spannowsky, *Effective Theories and Measurements at Colliders*, *Phys. Lett. B* **740** (2015) 8–15, [[arXiv:1408.5147](#)].
- [39] S. Dittmaier, A. Huss, and G. Knippen, *Next-to-leading-order QCD and electroweak corrections to WWW production at proton-proton colliders*, *JHEP* **09** (2017) 034, [[arXiv:1705.03722](#)].
- [40] T. Binoth, G. Ossola, C. G. Papadopoulos, and R. Pittau, *NLO QCD corrections to tri-boson production*, *JHEP* **06** (2008) 082, [[arXiv:0804.0350](#)].
- [41] J. Alwall, R. Frederix, S. Frixione, V. Hirschi, F. Maltoni, O. Mattelaer, H. S. Shao, T. Stelzer, P. Torrielli, and M. Zaro, *The automated computation of tree-level and next-to-leading order differential cross sections, and their matching to parton shower simulations*, *JHEP* **07** (2014) 079, [[arXiv:1405.0301](#)].
- [42] A. Alloul, N. D. Christensen, C. Degrande, C. Duhr, and B. Fuks, *FeynRules 2.0 - A complete toolbox for tree-level phenomenology*, *Comput. Phys. Commun.* **185** (2014) 2250–2300, [[arXiv:1310.1921](#)].
- [43] **CMS** Collaboration, H. Weber, *Slides on the observation of triple heavy boson production*, .
- [44] **CMS** Collaboration, A. Sirunyan et al., *Identification of heavy-flavour jets with the CMS detector in pp collisions at 13 TeV*, *JINST* **13** (2018), no. 05 P05011, [[arXiv:1712.07158](#)].
- [45] **ATLAS** Collaboration, M. Aaboud et al., *ZZ $\rightarrow \ell^+\ell^-\ell'^+\ell'^-$ cross-section measurements and search for anomalous triple gauge couplings in 13 TeV pp collisions with the ATLAS detector*, *Phys. Rev. D* **97** (2018), no. 3 032005, [[arXiv:1709.07703](#)].
- [46] M. Cepeda et al., *Report from Working Group 2: Higgs Physics at the HL-LHC and HE-LHC*, *CERN Yellow Rep. Monogr.* **7** (2019) 221–584, [[arXiv:1902.00134](#)].
- [47] F. Bishara, J. Brod, P. Uttayarat, and J. Zupan, *Nonstandard Yukawa Couplings and Higgs Portal Dark Matter*, *JHEP* **01** (2016) 010, [[arXiv:1504.04022](#)].

- [48] R. A. Porto and A. Zee, *The Private Higgs*, *Phys. Lett. B* **666** (2008) 491–495, [[arXiv:0712.0448](#)].
- [49] G. F. Giudice and O. Lebedev, *Higgs-dependent Yukawa couplings*, *Phys. Lett. B* **665** (2008) 79–85, [[arXiv:0804.1753](#)].
- [50] M. Bauer, M. Carena, and K. Gemmler, *Flavor from the Electroweak Scale*, *JHEP* **11** (2015) 016, [[arXiv:1506.01719](#)].
- [51] M. Bauer, M. Carena, and K. Gemmler, *Creating the fermion mass hierarchies with multiple Higgs bosons*, *Phys. Rev. D* **94** (2016), no. 11 115030, [[arXiv:1512.03458](#)].
- [52] J. Ellis, *TikZ-Feynman: Feynman diagrams with TikZ*, *Comput. Phys. Commun.* **210** (2017) 103–123, [[arXiv:1601.05437](#)].